



Nanoscale

**Click Catalysis and DNA Conjugation using a Nanoscale
DNA/Silver Cluster Pair**

Journal:	<i>Nanoscale</i>
Manuscript ID	NR-ART-07-2024-002938.R1
Article Type:	Paper
Date Submitted by the Author:	18-Aug-2024
Complete List of Authors:	Setzler, Caleb; Furman University, Chemistry Petty, Jeffrey; Furman University,

SCHOLARONE™
Manuscripts

ARTICLE

Received 00th January 20xx,
Accepted 00th January 20xx
DOI: 10.1039/x0xx00000x

Click Catalysis and DNA Conjugation using a Nanoscale DNA/Silver Cluster Pair

Caleb J. Setzler^a and Jeffrey T. Petty^{a,*}

DNA-bound silver clusters are most readily recognized by their strong fluorescence that spans the visible and near-infrared regions. From this suite of chromophores, we chose a green-emitting Ag_{10}^{6+} bound with $\text{C}_4\text{AC}_4\text{TC}_3\text{GT}_4$ and describe how this DNA/cluster pair is also a catalyst. A DNA-tethered alkyne conjugates with an azide via cycloaddition, an inherently slow reaction that is facilitated through the joint efforts of the cluster and DNA. The Ag_{10}^{6+} is the catalytic core in this complex, and it has three distinguishing characteristics. It facilitates cycloaddition while preserving its stoichiometry, charge, and spectra. It also acidifies its nearby alkyne to promote H/D exchange, suggesting a silver-alkyne complex. Finally, it is markedly more efficient when compared with related multinuclear DNA-silver complexes. The Ag_{10}^{6+} is trapped within its $\text{C}_4\text{AC}_4\text{TC}_3\text{GT}_4$ host, which governs catalytic activity in two ways. The DNA has orthogonal functional groups for both the alkyne and cluster, and these can be systematically separated to quench the click reaction. It is also a polydentate ligand that imprints an elongated shape on its cluster adduct. This extended structure suggests that DNA may pry apart the cluster to open coordination sites for the alkyne and azide reactants. These studies indicate that this DNA/silver cluster pair work together with catalysis directly driven by the silver cluster and indirectly guided by the DNA host.

Introduction

Size dictates the chemical and optical properties of noble metal nanomaterials, with distinctive behaviors emerging at nanometer scales.¹ For example, while gold in its bulk form is inert, its nanoparticles catalyze CO oxidation with a sharp 100-fold jump in efficiency for sizes ≤ 6 nm.^{2,3} These small nanoparticle are active because high surface areas expose coordination sites for exogenous reagents.⁴ This surface chemistry and catalysis is now more precisely controlled using noble metal nanoclusters.^{5,6} These are more precisely described as nanoscale molecules because they have a well-defined number of metals and ligands, organized as a metal core in a ligand shell.⁷ Now, size becomes a less relevant metric, and stoichiometry, structure, charge, and coordination environment dictate catalytic efficiency.⁸ Their catalysis is being studied and optimized through a fruitful collaboration of experimental and theoretical studies. A suite of synthetic methods can manipulate both the metal core and ligand shell at the atomic level.⁹ X-ray diffraction along with a diverse set of analytical tools atomically map these complexes.¹⁰ High-level theoretical calculations develop models to understand and optimize catalysis.¹¹ Here, we describe a nanoscale molecule comprised of a silver cluster within DNA, and this complex collectively catalyzes a cycloaddition reaction.

Transition metal cations are the linchpin of alkyne-azide cycloadditions because they catalyze these click reactions with rates that are 10^7 – 10^8 faster rates faster than the original Huisgen reaction.^{12–15} These catalyzed reactions are efficient at room temperature and in dilute solutions and are consequently used to link modular units and synthesize novel nanomaterials.^{16–19} A metal center facilitates stepwise annulation by coordinating an alkyne and

azide in its open sites.²⁰ This metal also activates these pendant ligands because it is an electrophile. For example, Cu^+ coordinates across alkyne π -bonds to withdraw electron density and acidify the terminal proton.¹⁵ A nucleophilic acetylide then attacks its neighboring azide, and the resulting C–N bond sets the foundation for an eventual triazole ring closure.¹³ While a single Cu^+ facilitates alkyne-azide cycloadditions, multinuclear complexes are more efficient. Two copper coordination sites are supported by kinetic studies that establish a second-order rate law with respect to copper.²¹ A dimeric Cu(I) catalyst is supported because a copper acetylide assembles with a Cu(I) complex and exchanges ^{63}Cu and ^{65}Cu isotopes.²² The pendant ligands freely migrate between the two coordination centers. The diverse end-on and side-on coordination modes of copper acetylides may underlie this enhanced activity because these interlinked complexes readily evolve to copper-triazole intermediates.^{23–25} To precisely control metal stoichiometry, molecular and nanoscale complexes have been synthesized.

Click reactions are widely used because they can be adapted and optimized for diverse reaction conditions, so these ‘black box’ approaches have motivated the search for more precisely defined catalysts.^{19, 26–28} For example, di-nuclear Cu^+ complexes are bridged by a bidentate carbene and labile acetate, and these complexes are effective homogeneous catalysts in a range of solvents.²⁹ Larger nanoscale molecules offer new opportunities to explore metal stoichiometry, structure, and coordination environment. One such nanocluster complex incorporates eight Cu^+ that are internally linked by acetylides and peripherally capped by carbenes.³⁰ The acetylides link coppers via both σ and π bonds, and the complex fluctuates with rapidly exchanging ligands. A Cu_{20} complex is concentrically organized around a partially reduced Cu_4^{2+} core with an outer shell having 12 acetylide ligands bridging 16 Cu^+ .³¹ The acetylides chemically exchange with exogenous alkynes to yield a mixture of triazole products. A Cu_{58} cluster is a click catalyst whose activity is enhanced by excising a single copper atom.³² This Cu_{57}

^a Department of Chemistry, Furman University, Greenville, SC, USA 29613

Supplementary Information available: [details of any supplementary information available should be included here]. See DOI: 10.1039/x0xx00000x

may be more active because the coppers and ligands around the vacated site reorganize. Mixed Au/Cu and Ag/Cu clusters reveal that electronic synergism facilitates alkyne/azide annulations.^{33, 34}

Besides Cu(I), other transition metals catalyze click reactions, and we consider a silver molecule.^{13, 35, 36} Again highlighting size dependent properties, these molecular forms of silver are fluorophores that are $\sim 10^{10}$ and $\sim 10^2$ brighter than bulk and nanoparticle forms of silver, respectively.^{37, 38} These fluorophores have diverse spectra that are revealed using DNA.³⁹ Single-stranded oligonucleotides coordinate silvers via their electron-rich, heterocyclic nucleobases, and multiple nucleobases frame binding pockets for a specific multinuclear cluster. DNA is programmable because its sequence and structure encode specific chromophores with spectra that span the visible and near-infrared and brightnesses that vary by $\sim 10^3$.^{40, 41} Here, we consider this spectroscopic DNA code from a chemical perspective. Silver clusters are protected within their DNA shell, but this matrix is permeable, as illustrated by cluster reactions with oxidizing and reducing agents.⁴²⁻⁴⁵ Here, we study a DNA/silver cluster pair that catalyzes alkyne-azide cycloadditions, a favored and selective reaction that is not perturbed by the diverse functional groups in DNA.⁴⁶ We first describe the DNA scaffold that shares both a silver cluster and an alkyne. The DNA-tethered alkyne reacts with azides without changing the nearby cluster, and a covalent triazole linkage was confirmed by etching the cluster from its DNA matrix. The cluster/DNA complex in D₂O reveals that the cluster acidifies its neighboring alkyne, possibly via a silver-alkyne complex. The click reaction efficiency depends on the cluster-alkyne proximity, which was controlled by inserting thymine spacers in the DNA strand. The solution pH also regulates reaction efficiency. Collectively, these experiments show how a DNA/silver cluster pair work together to catalyze alkyne-azide cycloadditions.

Experimental

Synthesis: The desalted oligonucleotides C₄AC₄TC₃GT₄ and Hx-C₄AC₄TC₃GT₄, where Hx is 1-hexyne attached at the 5' phosphate, were purchased from Integrated DNA Technologies and dissolved in deionized water before use. Molar extinction coefficients were calculated based on the nearest-neighbor approximation,⁴⁷ and the concentrations of these DNA stock solutions were determined using the Lambert – Beer law. In a typical synthesis, a 150 μ L sodium cacodylate buffer solution (1 mM, pH = 7) that contained 30 μ M C₄AC₄TC₃GT₄ (**1**) and 300 μ M AgNO₃ (10 molar equivalents:1). The mixture was first heated (~ 80 °C) for 5 min, then cooled to room temperature. An aqueous solution of NaBH₄ was added (5 molar equivalents:1) and then vortexed. The buffers were acetic acid/acetate (pH = 5), cacodylic acid/cacodylate (pH = 6-7), and boric acid/borate (pH = 7.5 and 8). The azides were N₃-C₃H₆-NH₂, N₃-C₆H₁₂O₂-C₁₀H₁₆N₃O₂S (Lumiprobe) and N₃-C₃H₆-OH (Synthonix). D₂O (Cambridge Isotopes) was used for H/D exchange.

Optical Characterization: Absorption spectra of DNA-Ag cluster conjugates were collected on a Cary 50 UV-Vis spectrophotometer (Varian), and steady-state emission spectra were collected on a Fluoromax-3 spectrofluorometer (Jobin-Yvon Horiba). Fluorescence quantum yields (QY) were measured by following well-established protocols using fluorescein as the standard (QY = 95%).⁴⁸ Time-correlated single photon counting measured the fluorescence lifetimes and anisotropies of these nanoclusters. Samples were excited by a pulsed 470-nm laser (PicoQuant) at a rate of 20 MHz using a FluoTime 300 (PicoQuant). The excitation beam was vertically polarized, and its power was fine-tuned to achieve a detection rate of fewer than 5 photons per 100 pulses ($< 5 \times 10^5$ Hz). The emission

was collected at a right-angle geometry with the emission polarizer set to the magic angle ($\sim 55^\circ$), and spectrally filtered using the monochromator. The instrument response function (IRF) was collected using colloidal silica (Aldrich), and the FWHM of the IRF was ~ 150 ps. The kinetics of fluorescence decay were extracted through IRF deconvolution fitting of the measured decay (EasyTau). The fluorescence anisotropy measurements were made using vertically (V) polarized excitation along with vertically (V) or horizontally (H) polarized emission.⁴⁹ The G-factor accounts for the detection efficiency of vertically and horizontally polarized emission and was measured using Fluorescein. The fluorescence decays under two different configurations, $I_{VV}(t)$ and $I_{VH}(t)$, were deconvolved with the IRF to calculate the anisotropy decay, $r(t)$, and rotational correlation time, τ_c (EasyTau).

Mass Spectrometry: The stoichiometry and charge of DNA-Ag cluster conjugates were characterized by electrospray ionization mass spectrometry (Q-TOF G2-S, Waters). DNA-silver clusters were dialyzed to remove low molecular impurities such as Na⁺. Samples were diluted with 100X volumes of 1 mM ammonium acetate and then reconcentrated by centrifugal dialysis using a 2 kDa cutoff filters (VivaSpin 20). Samples were diluted to ~ 0.3 μ M with 1 mM ammonium acetate and then infused via a syringe pump operated at 20 μ L/min. The spectra were collected in the negative ion mode with a capillary voltage of -2.7 kV, a sampling cone voltage of -15 V, an extraction cone voltage of 10 V, a cone gas flow of 45 L/h, and a desolvation gas flow of 450 L/h. The source temperature was 80 °C, and the desolvation temperature was 150 °C. Mass calibration was performed using aggregates of sodium iodide in the 400 < m/z < 2000 range. The spectra were analyzed using MassLynx V4.1.

Results

Neighbors in Shared DNA Scaffold: C₄AC₄TC₃GT₄ (**1**) assembles a silver cluster and alkyne via two distinct binding sites (Figure 1A). This sequence was chosen because it selectively forms a single silver chromophore with $\lambda_{ex}/\lambda_{em} = 490/555$ nm, and its multidentate binding site has been characterized by varying the DNA sequence (Figure 1B).⁵⁰ The four thymines at the 3' terminus can be removed, however, shorter variants of C₄AC₄TC₃G no longer favor the green emitting cluster, indicating that this 14-nucleobase tract is the minimal, core binding site.^{43, 50-52} This sequence folds around the cluster with the central thymine functioning as a hinge.⁴⁹ The DNA was further modified with a 1-hexyne at its 5' phosphate, and this covalently modified strand is henceforth referred to as **Hx-1**. In summary, C₄AC₄TC₃GT₄ (**1**) is a scaffold that shares an alkyne and a green-emitting silver cluster. The cluster is a silver molecule that was characterized using its mass and optical spectra.

Hx-1 mimicked **1** because it formed the same silver molecule, whose stoichiometry and charge were measured by electrospray ionization mass spectrometry (Figures 1C and 1S and Table 1S). As with the parent strand, **Hx-1** was combined with Ag⁺, which were chemically reduced to yield a range of adducts with 4-10 silvers. Ag₁₀ dominated, and it is a charged adduct that partially neutralizes the DNA.^{38, 49, 50, 53} **Hx-1**/Ag₁₀ complexes with net -4 and -5 charges were identified, each with characteristic isotopic distributions due to the 51.8% ¹⁰⁷Ag : 48.2% ¹⁰⁹Ag mixture in naturally occurring silver (Figure 1C-inset and 1S). The M/Z values and the intensities of 49 isotopologue peaks were analyzed to yield the molecular formulas [(C₁₇₅H₂₂₁N₅₃O₁₁₃P₁₈)⁻¹⁰(Ag₁₀)⁶⁺]⁻⁴ and [(C₁₇₅H₂₂₀N₅₃O₁₁₃P₁₈)⁻¹¹(Ag₁₀)⁶⁺]⁻⁵ (Table 1S).⁵³ Without the silver adduct, the -4 and -5 charged strands alone would have H₂₂₇ and H₂₂₆, respectively, so each complex is missing 6 H⁺. The reason for this deficit lies with the

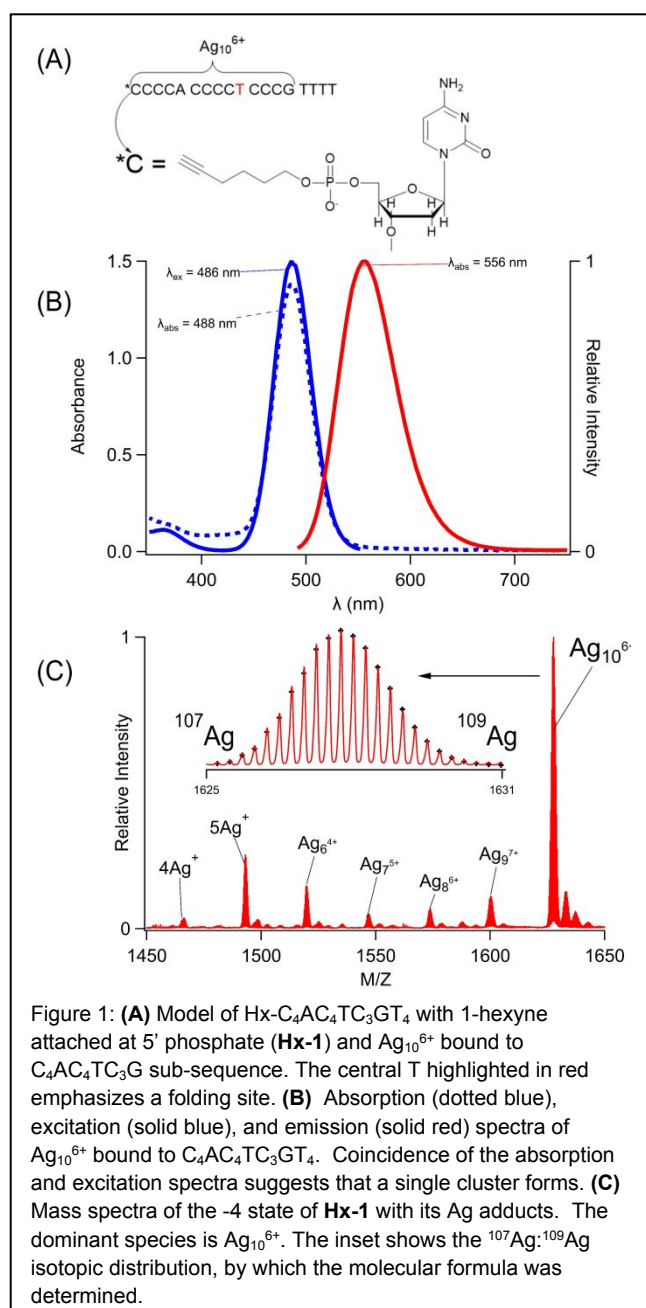


Figure 1: (A) Model of Hx-C₄AC₄TC₃GT₄ with 1-hexyne attached at 5' phosphate (Hx-1) and Ag₁₀⁶⁺ bound to C₄AC₄TC₃G sub-sequence. The central T highlighted in red emphasizes a folding site. (B) Absorption (dotted blue), excitation (solid blue), and emission (solid red) spectra of Ag₁₀⁶⁺ bound to C₄AC₄TC₃GT₄. Coincidence of the absorption and excitation spectra suggests that a single cluster forms. (C) Mass spectra of the -4 state of Hx-1 with its Ag adducts. The dominant species is Ag₁₀⁶⁺. The inset shows the ¹⁰⁷Ag:¹⁰⁹Ag isotopic distribution, by which the molecular formula was determined.

phosphate backbone. It acts like a buffer because its H⁺ are labile and displaced by the cationic silver cluster. The 6 fewer H⁺ suggests that the cluster is Ag₁₀⁶⁺. Both ions had Ag₁₀⁶⁺ adducts, consistent with a cluster that dictates protonation of the phosphate backbone. Oxidation states of other DNA-bound silver clusters have been measured by both mass spectrometry in the gas phase and by XANES measurements in solution, yielding the same charge.⁵⁴ Based on its +6 oxidation state, the Ag₁₀⁶⁺ has 4 Ag⁰, which are responsible for its green fluorescence.⁵⁵ The optical spectra are described next.

The coordination environment in Hx-1 was further interrogated using the absorption and fluorescence spectra of the Ag₁₀⁶⁺ adduct. This chromophore is a sensitive reporter because it has diverse spectra, ranging from a weakly emissive, λ_{max} = 400 nm chromophore to a 60-fold brighter, λ_{max} = 490 nm fluorophore.^{56, 57} Given these large changes, the Ag₁₀⁶⁺ spectra can discern

differences between its 1 and Hx-1 hosts (Figure 2S). The absorption spectra have similar λ_{max} values and absorbances, thus indicating that the clusters reside in comparable binding sites and form with similar efficiencies. The absorption and excitation maxima overlap, suggesting that a single cluster develops within their respective binding sites. The emission spectra have the same λ_{max} = 556 nm, and the fluorescence quantum yields are similar with 24 ± 4% for 1/Ag₁₀⁶⁺ and 30 ± 4% for Hx-1/Ag₁₀⁶⁺. The respective intensity-weighted average fluorescence lifetimes are 2.05 ± 0.03 ns and 2.23 ± 0.04 ns, again supporting similar electronic environments. The fluorescence decays were further utilized to compare the shapes of the DNA-cluster complexes. During fluorescence relaxation, the emission depolarizes as the complexes rotate to yield rotation correlation times of 2.50 ± 0.05 ns and 2.64 ± 0.09 ns using the strands without and with the hexyne, respectively. These times are similar to the heterodimeric (C₄AC₄T + C₃GT₄)/Ag₁₀⁶⁺ complex and suggests that both Hx-1 and 1 are folded at the central thymine.^{49, 58} Thus, the mass and optical spectra demonstrate that the same Ag₁₀⁶⁺ fluorophore forms with both Hx-1 and 1.

Catalytic Cluster: The Ag₁₀⁶⁺ and hexyne are nearby in their shared DNA scaffold yet appear to be decoupled, as the same Ag₁₀⁶⁺ adduct has nearly identical spectra using C₄AC₄TC₃GT₄ without and with 1-hexyne appended. However, from the vantage of the alkyne, it now reacts with azides, a reaction that is prohibitively slow without the cluster.¹² Two smaller aliphatic and one larger biotin-based azides were used: N₃-C₃H₆-NH₂, N₃-C₃H₅-OH, and N₃-C₆H₁₂O₂-C₁₀H₁₆N₃O₂S (Biotin) (Figures 2A, 2B, and 3S). Azide complexes with Hx-1/Ag₁₀⁶⁺ were identified in the mass spectra, and their formulas were derived from the isotopologue peaks in the -4 and -5 states of these complexes. Based on the M/Z values and the isotopologue intensity distributions, the following formulas were derived for the -4 and -5 charged ions of each complex: [(C₁₇₈H₂₂₉O₁₁₃N₅₇P₁₈)⁻¹⁰(Ag₁₀⁶⁺)⁻⁴] and [(C₁₇₈H₂₂₈O₁₁₃N₅₇P₁₈)⁻¹¹(Ag₁₀⁶⁺)⁻⁵] for N₃-C₃H₆-NH₂ (Table 2S), [(C₁₇₈H₂₂₈O₁₁₄N₅₆P₁₈)⁻¹⁰(Ag₁₀⁶⁺)⁻⁴] and [(C₁₇₈H₂₂₇O₁₁₄N₅₆P₁₈)⁻¹¹(Ag₁₀⁶⁺)⁻⁵] for N₃-C₃H₅-OH (Table 3S), and [(C₁₉₁H₂₄₉O₁₁₇N₅₉SP₁₈)⁻¹⁰(Ag₁₀⁶⁺)⁻⁴] and [(C₁₉₁H₂₄₈O₁₁₇N₅₉SP₁₈)⁻¹¹(Ag₁₀⁶⁺)⁻⁵] for N₃-C₆H₁₂O₃-Biotin (Table 4S). These formulas show Ag₁₀⁶⁺ is preserved when the DNA-tethered hexyne reacts with the azides. Furthermore, the coordination sites are conserved, as reported by similar absorption spectra (Figure 4S). Our subsequent results focus on N₃-C₃H₆-NH₂. While Hx-1 hosts other silver adducts, only the Hx-1/Ag₁₀⁶⁺ complex associates with this azide, and the efficiency of labelling was calculated by integrating peak areas for all DNA/silver complexes (Figure 2C, red vs. black peaks). The integrity of the N₃-C₃H₆-NH₂/DNA/cluster complex was challenged by diluting a sample with 100X volumes of solution to dissociate weakly bound complexes and then reconcentrated using centrifugal dialysis. The absorption spectra remain consistent with the same λ_{max} and absorbance, indicating that the cluster is stable in its azide-tagged DNA host (Figure 5S). Also, the reaction efficiencies are similar, so we conclude that only the DNA-bound Ag₁₀⁶⁺, not leached Ag⁰/Ag⁺, facilitate the reaction (Figure 5S).^{31, 59} Thus, the DNA-bound cluster facilitates but remains unchanged by alkyne-azide coupling.

Ag₁₀⁶⁺ was used as a starting point to create other possible silver-laden DNA catalysts.⁴⁴ This chromophore has 4 Ag⁰ that provide a photochemical handle by which Ag₁₀⁶⁺ can be selectively excited and degraded by irradiating at 490 nm.⁴⁴ The photodestruction quantum yield ~10⁻⁴, so the sample was irradiated for an extended period. As the Ag₄⁰ absorption at 490 nm diminished, a new higher

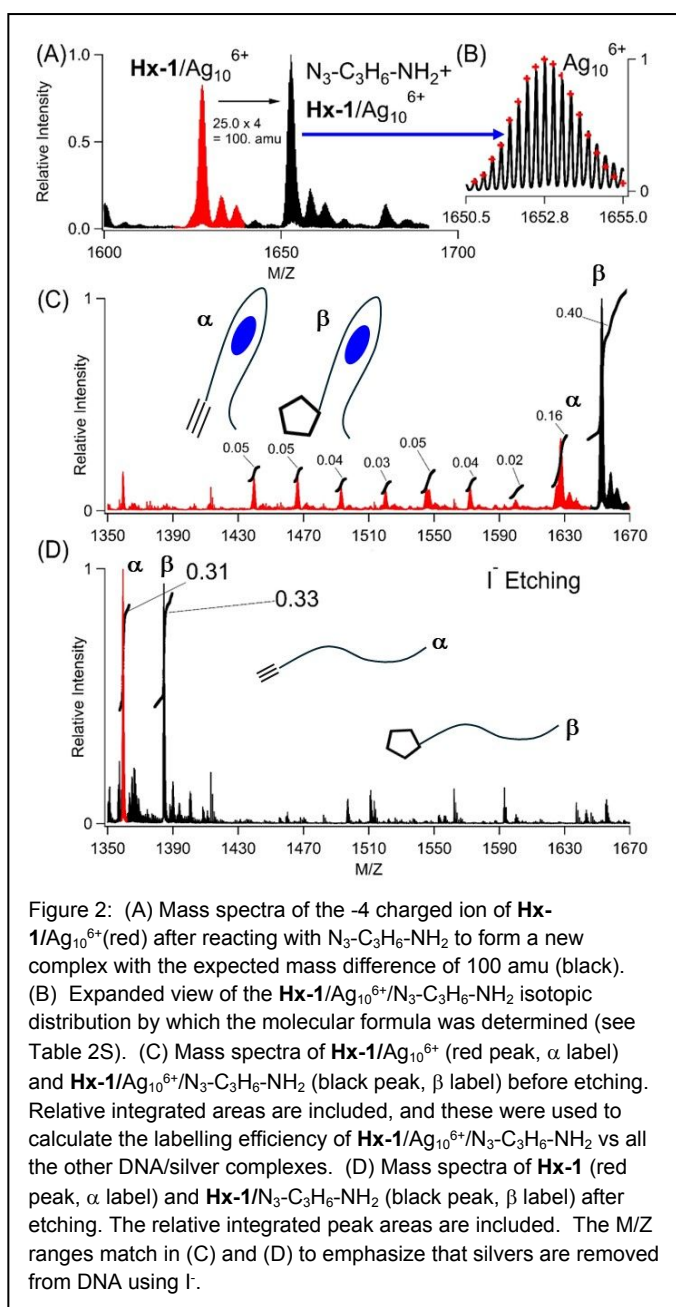


Figure 2: (A) Mass spectra of the -4 charged ion of **Hx-1**/ Ag_{10}^{6+} (red) after reacting with $\text{N}_3\text{-C}_3\text{H}_6\text{-NH}_2$ to form a new complex with the expected mass difference of 100 amu (black). (B) Expanded view of the **Hx-1**/ Ag_{10}^{6+} / $\text{N}_3\text{-C}_3\text{H}_6\text{-NH}_2$ isotopic distribution by which the molecular formula was determined (see Table 2S). (C) Mass spectra of **Hx-1**/ Ag_{10}^{6+} (red peak, α label) and **Hx-1**/ Ag_{10}^{6+} / $\text{N}_3\text{-C}_3\text{H}_6\text{-NH}_2$ (black peak, β label) before etching. Relative integrated areas are included, and these were used to calculate the labelling efficiency of **Hx-1**/ Ag_{10}^{6+} / $\text{N}_3\text{-C}_3\text{H}_6\text{-NH}_2$ vs all the other DNA/silver complexes. (D) Mass spectra of **Hx-1** (red peak, α label) and **Hx-1**/ $\text{N}_3\text{-C}_3\text{H}_6\text{-NH}_2$ (black peak, β label) after etching. The relative integrated peak areas are included. The M/Z ranges match in (C) and (D) to emphasize that silvers are removed from DNA using I^- .

energy transition due to Ag_2^0 developed at 340 nm (Figure 6SC).⁶⁰⁻⁶⁴ However, this photochemical change is more interesting than a simple $\text{Ag}_4^0 \rightarrow \text{Ag}_2^0$ conversion because the mass spectra identified two distributions of photoproducts (Figure 6SA and 6SB). As expected from the $\lambda = 490 \rightarrow 340$ nm shift, the DNA coordinated Ag_2^0 , but multiple clusters with different number of Ag^+ were identified - Ag_6^{4+} , Ag_5^{5+} (dominant species), Ag_8^{6+} , and Ag_9^{7+} . Irradiation also produced purely oxidized 4 and 5 Ag^+ adducts, which are devoid of Ag^0 and thus spectrally silent. We used a sample irradiated for a short time to collectively evaluate how the DNA-bound Ag^+ , Ag_2^0 , and Ag_4^0 species react with $\text{N}_3\text{-C}_3\text{H}_6\text{-NH}_2$. Despite their high abundance and redundancy, the Ag^+ and Ag_2^0 complexes did not react and only the Ag_{10}^{6+} adduct promoted alkyne-azide coupling (see red peaks in Figure 6SA). Thus, the alkyne reaction with azides is specific for Ag_{10}^{6+} , and the reaction

products were characterized by extracting the cluster from the DNA.

Three experiments indicate that Ag_{10}^{6+} facilitates cycloaddition to yield a covalently linked triazole, as shown using $\text{N}_3\text{-C}_3\text{H}_6\text{-NH}_2$ with **Hx-1**/ Ag_{10}^{6+} . One, this azide remained integrated with the DNA after Ag_{10}^{6+} was removed. Silver clusters are etched by I^- , presumably because AgI(s) has such a small $K_{sp} = 10^{-18}$. With 1 equivalent of iodide:silver, the Ag_{10}^{6+} absorption at 490 nm was quenched, signalling that silvers were no longer associated with the DNA (Figure 7S). In support, two strands devoid of silvers emerged in the mass spectra: **Hx-1** alone and with $\text{N}_3\text{-C}_3\text{H}_6\text{-NH}_2$ (Figure 2C). The latter supports alkyne-azide cycloaddition between the DNA-tethered alkyne and $\text{N}_3\text{-C}_3\text{H}_6\text{-NH}_2$, a union that is selective and strongly thermodynamically favored ($\Delta G \sim -45$ kcal).^{12, 16} The areas of these two peaks were integrated to give a labelling efficiency of 52%, comparable to the 48% before etching (Figures 2D vs 2C). Inactive DNA-bound Ag^+ and Ag_2^0 adducts are further supported by the low labelling efficiency of a photolyzed sample (Figure 8SB). Two, $\text{N}_3\text{-C}_3\text{H}_6\text{-NH}_2$ was added to **1**/ Ag_{10}^{6+} but does not form a stable complex (Figure 9S). Three, after reaction with $\text{N}_3\text{-C}_3\text{H}_6\text{-NH}_2$ and then I^- , the denuded DNA strands were dialyzed against 100X and 10000X volumes of solution (Figure 10S). The relative amounts of unlabelled and labelled DNA did not change, further supporting a stable, covalently linked triazole.

Enhanced Acidity: **Hx-1** becomes more acidic due to its Ag_{10}^{6+} adduct, and the acidic site was identified using H/D exchange. The DNA/cluster complex has nearly identical absorption spectra in H_2O and D_2O , suggesting that the clusters formed with similar efficiencies in the same coordination environment (Figure 11S). To isolate the effect of the cluster, it was extracted from its DNA host using CN^- , which readily complexes with Ag^+ to form Ag(CN)_2^- . With $K = 10^{18}$, this CN^- and Ag(CN)_2^- complex ion are expected to overwhelm any affinity of DNA for silvers, as supported by quenched Ag_{10}^{6+} absorption (Figures 11S). This sample was finally washed with 100 volumes of H_2O (Figure 3A-Case I). Swapping D_2O with this large amount of H_2O will reprotonate the plethora of natural acidic and basic functional groups in a DNA.⁴⁷ However, the alkyne appended onto **1** is inherently more basic with $\text{pK}_a \sim 26$, thus resisting reprotonation.¹² Mass spectra show denuded strands with net -5 , -4 , and -3 charges, and the M/Z values and the isotope distributions of the isotopologue peaks show that the molecular formula has exchanged a hydrogen with deuterium, i.e. $\text{C}_{175}\text{H}_{230}\text{DN}_{53}\text{O}_{113}\text{P}_{18}$ (DNA with zero net charge) (Figures 3B and 12SA and Table 5S). Three other experiments firmly established the alkyne deuteration site. First, **Hx-1**/ Ag_{10}^{6+} was prepared in H_2O , and the mass spectra show the expected fully protonated, bare DNA (Figures 3A-Case II and 12SB and Table 6S). Second, $\text{C}_4\text{AC}_4\text{TC}_3\text{GT}_4/\text{Ag}_{10}^{6+}$ without the hexyne was prepared in D_2O , yet the silver-free DNA is fully protonated (Figures 3A-Case III and 12SC and Table 7S). As a further control, **Hx-1** without Ag_{10}^{6+} in D_2O shows no deuteration (Figures 3A-Case IV and 12SD and Table 8S). These experiments suggest that Ag_{10}^{6+} coordinates with and acidifies its neighboring alkyne.

Reaction Efficiency: **Hx-1** anchors both the cluster and alkyne, and their proximity controls reaction efficiency. This DNA is modular because it can be lengthened to separate its two adducts. Thymine was inserted because they bind poorly with silvers and do not perturb a cluster coordination site.^{51, 52} **Hx-T_x-1** strands with $x = 0, 1, 2, 3$, and 4 thus hold the Ag_{10}^{6+} in its favored $\text{C}_4\text{AC}_4\text{TC}_3\text{G}$ binding site while still keeping the hexyne on the 5' terminus.

Considering DNA as a linear polymer, these longer strands progressively distanced the alkyne from its neighboring cluster. All five oligonucleotides formed the same Ag_{10}^{6+} adducts, whose

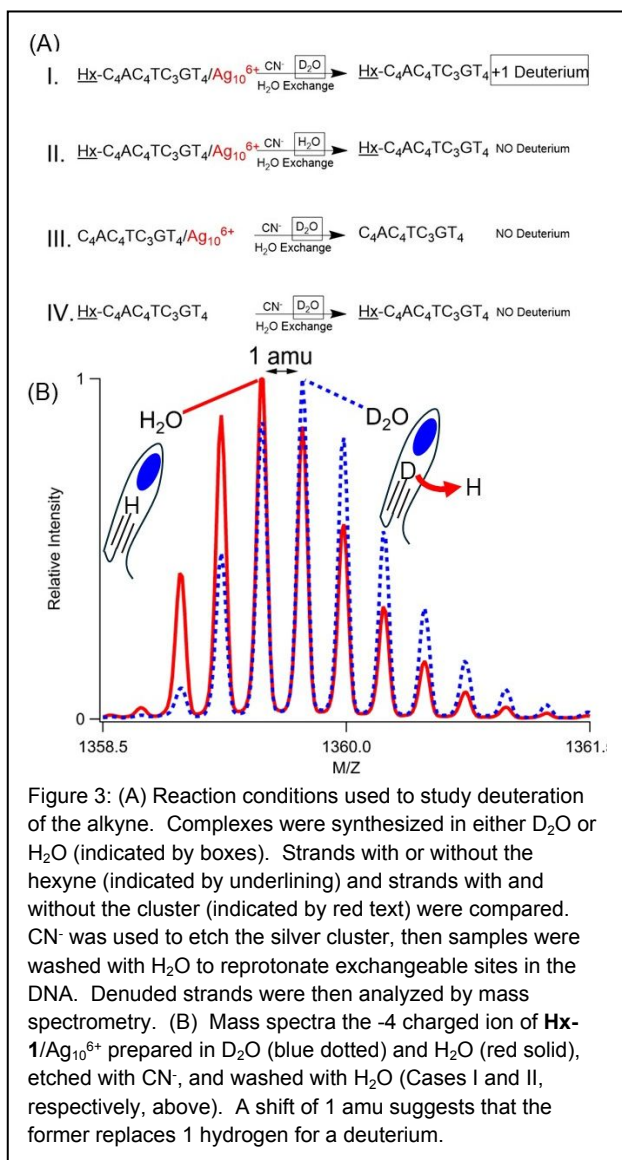


Figure 3: (A) Reaction conditions used to study deuteration of the alkyne. Complexes were synthesized in either D_2O or H_2O (indicated by boxes). Strands with or without the hexyne (indicated by underlining) and strands with and without the cluster (indicated by red text) were compared. CN^- was used to etch the silver cluster, then samples were washed with H_2O to reprotoate exchangeable sites in the DNA. Denuded strands were then analyzed by mass spectrometry. (B) Mass spectra the -4 charged ion of **Hx-1**/ Ag_{10}^{6+} prepared in D_2O (blue dotted) and H_2O (red solid), etched with CN^- , and washed with H_2O (Cases I and II, respectively, above). A shift of 1 amu suggests that the former replaces 1 hydrogen for a deuterium.

similar $\lambda_{\text{max}} \sim 490 \text{ nm}$ and absorbances suggest that the clusters developed with comparable efficiencies (Figure 13S). Thus, the added thymine were innocuous, and the cluster remained confined and thus progressively more distant from the 5'-terminal hexyne. These DNA/ Ag_{10}^{6+} complexes reacted differently with $\text{N}_3\text{-C}_3\text{H}_6\text{-NH}_2$, as the reaction efficiencies were highest without an added thymine ($x=0$ strand) but diminished as more thymine are added (Figures 4 and 14S). Thus, these results suggest the DNA is modular and can be lengthened to temper the click reaction.

Conditions relevant to click reactions were also considered. Oxidation of redox active metals can render incompetent catalysts.^{26,27} With **Hx-1**/ Ag_{10}^{6+} , solutions purged with O_2 vs. N_2 showed no differences in conversion, suggesting that O_2 does not affect the Ag_{10}^{6+} catalyst (Figure 15S).⁴² The solution pH can also influence a click reaction through deprotonation of terminal alkynes and reprotonation of Cu-triazolyl intermediates. Over the range from pH = 5-8.5, the same Ag_{10}^{6+} adducts formed with **Hx-1** with little variance in their optical spectra (Figures 16S and 17S).

However, strong differences emerge with addition of $\text{N}_3\text{-C}_3\text{H}_6\text{-NH}_2$. The conversion efficiency increases ~ 25 fold over this pH range, with a sharp jump at pH = 6-7. Enhanced reaction is also observed at higher pH for Cu(I) coordinated with benzimidazole ligands.⁶⁵ As with these polydentate amine-based ligands, DNA is rich reservoir of acidic and basic heteroatoms that may regulate deprotonation and reprotonation steps in a click reaction.⁶⁶

Discussion

Together, **Hx-1** and Ag_{10}^{6+} catalyze an alkyne-azide click reaction, and each component in this pair has distinct roles. The Ag_{10}^{6+} is the catalyst, and we discuss three of its characteristics – it is preserved while facilitating the click union, it acidifies its neighboring alkyne, and it is distinctly active compared to related complexes. The activity of this catalyst is regulated by the DNA host, which serves two roles – it segregates the cluster within the larger DNA host and it imprints an elongated cluster shape. We now discuss these five characteristics of this nanoscale catalyst.

Ag_{10}^{6+} unites a DNA-tethered alkyne with an azide without changing its stoichiometry, charge, and spectra. However, click

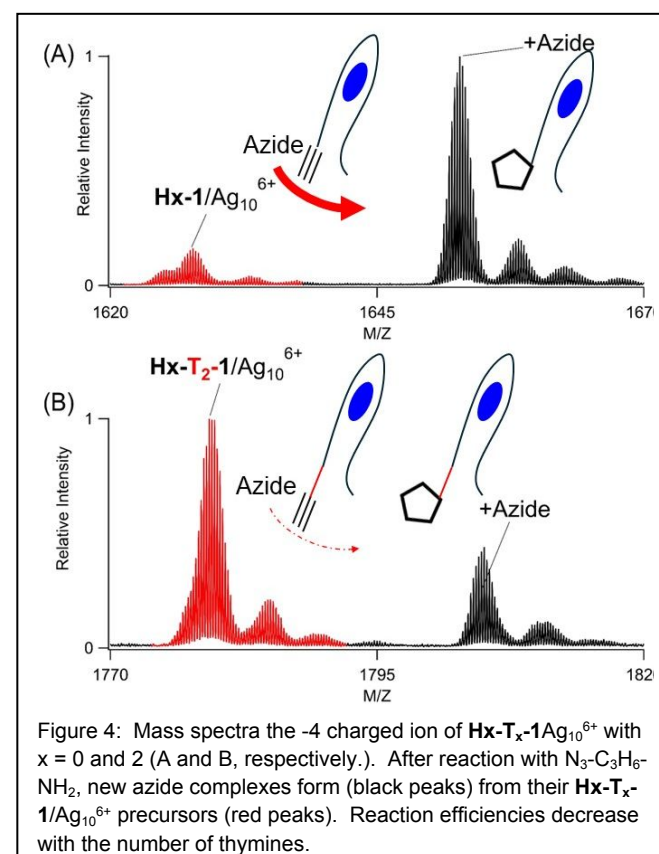


Figure 4: Mass spectra the -4 charged ion of **Hx-T_x-1**/ Ag_{10}^{6+} with $x = 0$ and 2 (A and B, respectively). After reaction with $\text{N}_3\text{-C}_3\text{H}_6\text{-NH}_2$, new azide complexes form (black peaks) from their **Hx-T_x-1**/ Ag_{10}^{6+} precursors (red peaks). Reaction efficiencies decrease with the number of thymine.

reactions conserve atoms, so mass spectra cannot distinguish whether an azide reacts with the alkyne or simply coordinates with silvers. To consider these two possibilities, iodide was added upon completing the reaction. This halide degrades the cluster to quench the Ag_{10}^{6+} absorption and strip the DNA of silvers. Two bare **Hx-1** strands are identified - without and with the azide. With the silver coordination sites now missing, we conclude that the azide is covalently linked as a triazole. In support, the **Hx-1**/azide conjugate survives 10,000X dilution, thus supporting a stable, covalent linkage that resists dissociation. Also, without the DNA-bound alkyne, **1**/ Ag_{10}^{6+} does not form a stable complex with azides. Thus, Ag_{10}^{6+}

catalyzes cycloaddition, and its role as a catalyst is suggested by studies in D₂O.

Transition metals catalyze alkyne-azide cycloadditions in steps, beginning with deprotonation of a terminal alkyne. Ag₁₀⁶⁺ may follow a similar catalytic path because it acidifies its neighboring alkyne, thereby effecting H/D exchange in D₂O. By analogy with other Cu(I) and Ag(I) catalysts, a deprotonated alkyne converts to a metal acetylide, a strong nucleophile that can attack an azide to set the first C-N bond for a triazole.^{36, 67} Further experiments are evaluating this proposed mechanism.¹² Beyond a mononuclear complex, silver acetylides can be multinuclear with both end-on and side-on coordination to give a rich and diverse array of structures.^{25, 68} To better understand the nuclearity of the Hx-1/Ag₁₀⁶⁺ catalyst, we studied pared down versions of this complex.

Relative to mononuclear complexes, multinuclear click catalysts are more effective, so smaller analogs of Hx-1/Ag₁₀⁶⁺ were studied. The 4 Ag⁰ in Ag₁₀⁶⁺ were selectively irradiated to yield DNA complexes with less Ag⁰ - Ag₂⁰ (Ag₆⁴⁺, Ag₇⁵⁺, Ag₈⁶⁺, and Ag₉⁷⁺) and purely Ag⁺ (3-5 Ag⁺) adducts. However, these multinuclear, derivatives of Ag₁₀⁶⁺ are incompetent catalysts, behaving as if the DNA were completely bare. They may be inactive because of their structure. Their wide distribution of silvers suggests that the preexisting Hx-1 binding site is indiscriminate and has little preference for a particular adduct. Thus, these photoproducts may be loosely bound with ill-defined structures, so they may be poor catalysts. We are searching for truncated oligonucleotides better suited for these photofragments. For example, complementary strands can shorten long DNA binding sites to favor smaller clusters.⁵⁷ Metal oxidation may also underlie the tepid activity of the Ag₂⁰ and Ag⁺ adducts with Hx-1. Dinuclear copper complexes have dynamic coordination environments whose ligands readily exchange because copper oxidation weakens π -backbonding and ligand coordination.^{22, 69} One avenue to better understand metal oxidation might be to change the balance of Ag⁺ and Ag⁰ in a cluster. Specifically, Ag₁₁⁷⁺ is also a green-emitting fluorophore like Ag₁₀⁶⁺, but it has an additional Ag⁺ that could alter the activity of this cluster.^{32, 42, 70} We are also studying other DNA/silver cluster complexes. In summary, Ag₁₀⁶⁺ is the catalytic core of the Hx-1/Ag₁₀⁶⁺ complex and has three characteristics: it joins the alkyne with azides via cycloaddition, it acidifies and possibly activates the alkyne, and it markedly more active than related DNA-silver complexes. The click reaction evolves within the confines of the Hx-1 scaffold, and we now discuss how it guides these reactions.

The green-emitting Ag₁₀⁶⁺ exists because it is trapped and shielded inside Hx-1, and this C₄AC₄TC₃G coordination site is a discrete unit in a larger DNA polymer. In addition, the DNA was further derivatized with 1-hexyne at its 5' terminal phosphate, yielding a dual-labeled Hx-1/Ag₁₀⁶⁺ conjugate. These adducts are independent and were separated by inserting thymines. Furthermore, these binding sites are independent, so the alkyne and cluster adduct can be separated by inserting thymines, neutral spacers that bind poorly with silver. With these longer Hx-T_x-1 strands, the cluster does not spill out of its binding site, as signified by the consistent mass and optical spectra for these variants. As the number of thymines increases, the click conversion efficiency drops. Considering the DNA to be a linear polymer, increasing distance between the alkyne and cluster thus tempers the click reaction with azides. Besides phosphates, specific nucleobases can also be alternate sites to derivatize a DNA. For example, X-ray diffraction studies show that the 3'-terminal adenine in (CACCTAGCGA)₂-Ag₁₆ is not associated with the cluster and can be labeled with peptides and proteins.^{71, 72} Also, fluorescence

anisotropy studies show that the central thymine in C₄AC₄TC₃GT₄ (1) is a folding site where the strand can be broken.⁴⁹ The resulting heterodimer reassembles to form the same green-emitting Ag₁₀⁶⁺ as the contiguous C₄AC₄TC₃GT₄. Thus, we suggest that specific sites could be derivatized in C₄AC₄TC₃GT₄/Ag₁₀⁶⁺ to better understand its click catalysis. DNA is not only a scaffold that tunes reaction efficiency but is also a polydentate ligand that shapes its cluster adduct.

Bare silver clusters have multiple interconverting isomers, and a DNA can select and favor specific isomers. For example, a single-stranded oligonucleotide coordinates a weakly emissive Ag₁₀⁶⁺ adduct, but this DNA hybridizes with a short complementary strand to now favor a strongly emissive Ag₁₀⁶⁺.⁵⁶ This switch reverses when the complement denatures. We now consider the shape of the Ag₁₀⁶⁺ adduct bound to Hx-1. This complex is a member of a larger class of Ag₄⁰-based chromophores with green emission whose structures have been considered from a variety of perspectives.^{38, 40, 55} EXAFS studies of a DNA-bound Ag₁₀⁶⁺ show limited metal-metal vs metal-DNA coordination when compared to a related weakly fluorescent cluster.^{54, 73} UV-based DNA footprinting identifies large segments of the DNA host that are protected from photodegradation by the Ag₁₀⁶⁺ adduct, again contrasting with localized binding and protection by a weakly fluorescent cluster.⁷⁴ Time-resolved infrared spectra show that the C₄AC₄TC₃GT₄ strand used in this study chelates its Ag₁₀⁶⁺ adduct using multiple nucleobases.⁷⁵ X-ray diffraction studies of a Ag₁₁⁷⁺ show a rod-like structure with distinct Ag₆ and Ag₅ subunits that follow the contour of the DNA polymer.⁷⁰ Quantum mechanical models predict cluster spectra based on rod-like shapes.^{38, 55} We propose that Ag₁₀⁶⁺ bound to Hx-1 also adopts an elongated shape and is dispersed within its DNA matrix, favoring metal-ligand over metal-metal coordination. An important question is the relative strength of nucleobase-silver coordination and competition with exogenous reagents, and prior studies indicate that reagents can penetrate and access open sites on the cluster.^{8, 32, 44, 45}

Conclusion

Single-stranded oligonucleotides encode the spectra of silver molecules via their sequence and structure, and this templated synthesis is illustrated by the C₄AC₄TC₃GT₄ strand which preferentially forms Ag₁₀⁶⁺. Besides being a strong fluorophore with green emission, this cluster also catalyzes click reactions between a DNA-tethered alkyne and azides. We conclude that DNA is a scaffold that guides catalysis in two ways. First, it segregates the cluster into a discrete, orthogonal binding pocket that leaves the larger DNA polymer open to be further functionalized. We hope to probe the nanoscale DNA/cluster catalyst by site specifically modifying the DNA. Second, DNA imprints the cluster shape and thus prescribes the coordination environment. We hope to modify the DNA polymer to fine-tune how click reagents access open coordination sites and bind with exposed silvers. Our overall conclusion is that silver molecules are effective click catalysts, and their activity can be directed by a DNA scaffold.

Author contributions

Jeffrey Petty and Caleb Setzler contributed equally to this work. Both authors conducted the experiments, analyzed the data, and wrote the manuscript. All authors have read and approved the final version of the manuscript.

Conflicts of interest

No conflicts to declare.

Data availability

The data supporting this article are included as part of the Supplementary Information.

Acknowledgements

The authors thank the National Science Foundation (CHE-1611451 and CHE-2002910) and the Furman Advantage program. This work was supported in part by the National Science Foundation EPSCoR Program under NSF Award No. OIA-1655740. Any opinions, findings, and conclusions or recommendations expressed in this material are those of the author(s) and do not necessarily reflect those of the National Science Foundation.

Notes and references

1. P. P. Edwards and J. M. Thomas, *Angewandte Chemie International Edition*, 2007, **46**, 5480-5486.
2. M. Haruta, T. Kobayashi, H. Sano and N. Yamada, *Chem. Lett.*, 2006, **16**, 405-408.
3. G. C. Bond and D. T. Thompson, *Gold Bulletin*, 2000, **33**, 41-50.
4. N. Lopez, T. V. W. Janssens, B. S. Clausen, Y. Xu, M. Mavrikakis, T. Bligaard and J. K. Nørskov, *Journal of Catalysis*, 2004, **223**, 232-235.
5. M. Brust, M. Walker, D. Bethell, D. J. Schiffrin and R. Whyman, *Journal of the Chemical Society, Chemical Communications*, 1994, DOI: 10.1039/C39940000801, 801-802.
6. R. L. Whetten, J. T. Khoury, M. M. Alvarez, S. Murthy, I. Vezmar, Z. L. Wang, P. W. Stephens, C. L. Cleveland, W. D. Luedtke and U. Landman, *Adv. Mater.*, 1996, **8**, 428-433.
7. R. Jin, *Nanoscale*, 2015, **7**, 1549-1565.
8. M. F. Matus and H. Häkkinen, *Nature Reviews Materials*, 2023, **8**, 372-389.
9. Y. Du, H. Sheng, D. Astruc and M. Zhu, *Chem. Rev.*, 2020, **120**, 526-622.
10. P. D. Jadzinsky, G. Calero, C. J. Ackerson, D. A. Bushnell and R. D. Kornberg, *Science*, 2007, **318**, 430-433.
11. O. Lopez-Acevedo, K. A. Kacprzak, J. Akola and H. Häkkinen, *Nat. Chem.*, 2010, **2**, 329-334.
12. F. Himo, T. Lovell, R. Hilgraf, V. V. Rostovtsev, L. Noodleman, K. B. Sharpless and V. V. Fokin, *J. Am. Chem. Soc.*, 2005, **127**, 210-216.
13. C. Wang, D. Ikhlef, S. Kahlal, J.-Y. Saillard and D. Astruc, *Coord. Chem. Rev.*, 2016, **316**, 1-20.
14. C. W. Tornøe, C. Christensen and M. Meldal, *The Journal of Organic Chemistry*, 2002, **67**, 3057-3064.
15. V. V. Rostovtsev, L. G. Green, V. V. Fokin and K. B. Sharpless, *Angewandte Chemie International Edition*, 2002, **41**, 2596-2599.
16. H. C. Kolb, M. G. Finn and K. B. Sharpless, *Angewandte Chemie International Edition*, 2001, **40**, 2004-2021.
17. D. Honcharenko, K. Druceikaite, M. Honcharenko, M. Bollmark, U. Tedebark and R. Strömberg, *ACS Omega*, 2021, **6**, 579-593.
18. N. Z. Fantoni, A. H. El-Sagheer and T. Brown, *Chem. Rev.*, 2021, **121**, 7122-7154.
19. S. I. Presolski, V. P. Hong and M. G. Finn, *Current Protocols in Chemical Biology*, 2011, **3**, 153-162.
20. J. E. Hein and V. V. Fokin, *Chem. Soc. Rev.*, 2010, **39**, 1302-1315.
21. V. O. Rodionov, V. V. Fokin and M. G. Finn, *Angewandte Chemie International Edition*, 2005, **44**, 2210-2215.
22. B. T. Worrell, J. A. Malik and V. V. Fokin, *Science*, 2013, **340**, 457-460.
23. B. F. Straub, *Chem. Commun.*, 2007, DOI: 10.1039/B706926J, 3868-3870.
24. M. Ahlquist and V. V. Fokin, *Organometallics*, 2007, **26**, 4389-4391.
25. A. K. Gupta and A. Orthaber, *Chem. Eur. J.*, 2018, **24**, 7536-7559.
26. M. G. Finn and V. V. Fokin, in *Catalysis without Precious Metals*, 2010, DOI: <https://doi.org/10.1002/9783527631582.ch10>, pp. 235-260.
27. V. O. Rodionov, S. I. Presolski, D. Díaz Díaz, V. V. Fokin and M. G. Finn, *J. Am. Chem. Soc.*, 2007, **129**, 12705-12712.
28. P. S. Donnelly, S. D. Zanatta, S. C. Zammit, J. M. White and S. J. Williams, *Chem. Commun.*, 2008, DOI: 10.1039/B719724A, 2459-2461.
29. R. Berg, J. Straub, E. Schreiner, S. Mader, F. Rominger and B. F. Straub, *Advanced Synthesis & Catalysis*, 2012, **354**, 3445-3450.
30. A. Makarem, R. Berg, F. Rominger and B. F. Straub, *Angewandte Chemie International Edition*, 2015, **54**, 7431-7435.
31. A. W. Cook, Z. R. Jones, G. Wu, S. L. Scott and T. W. Hayton, *J. Am. Chem. Soc.*, 2018, **140**, 394-400.
32. C. Dong, R.-W. Huang, A. Sagadevan, P. Yuan, L. Gutiérrez-Arzaluz, A. Ghosh, S. Nematullov, B.

- Alamer, O. F. Mohammed, I. Hussain, M. Rueping and O. M. Bakr, *Angewandte Chemie International Edition*, 2023, **62**, e202307140.
33. Y. Fang, K. Bao, P. Zhang, H. Sheng, Y. Yun, S.-X. Hu, D. Astruc and M. Zhu, *J. Am. Chem. Soc.*, 2021, **143**, 1768-1772.
34. J.-P. Gao, F.-Q. Zhang and X.-M. Zhang, *Advanced Science*, 2024, **n/a**, 2400377.
35. J. T. Petty, J. Zheng, N. V. Hud and R. M. Dickson, *J. Am. Chem. Soc.*, 2004, **126**, 5207-5212.
36. J. McNulty and K. Keskar, *European Journal of Organic Chemistry*, 2012, **2012**, 5462-5470.
37. O. A. Yeshchenko, I. M. Dmitruk, A. A. Alexeenko, M. Y. Losytskyy, A. V. Kotko and A. O. Pinchuk, *Physical Review B*, 2009, **79**, 235438.
38. D. Schultz, K. Gardner, S. S. R. Oemrawsingh, N. Markešević, K. Olsson, M. Debord, D. Bouwmeester and E. Gwinn, *Adv. Mater.*, 2013, **25**, 2797-2803.
39. A. González-Rosell, C. Cerretani, P. Mastracco, T. Vosch and S. M. Copp, *Nanoscale Adv.*, 2021, **3**, 1230-1260.
40. C. I. Richards, S. Choi, J.-C. Hsiang, Y. Antoku, T. Vosch, A. Bongiorno, Y.-L. Tzeng and R. M. Dickson, *J. Am. Chem. Soc.*, 2008, **130**, 5038-5039.
41. H. C. Yeh, J. Sharma, J. J. Han, J. S. Martinez and J. H. Werner, *Nano Lett*, 2010, **10**, 3106-3110.
42. J. T. Petty, D. Lewis, S. Carnahan, D. Kim and C. Couch, *J. Phys. Chem. B*, 2022, **126**, 3822-3830.
43. J. T. Petty, S. Carnahan, D. Kim and D. Lewis, *J. Chem. Phys.*, 2021, **154**, 244302.
44. C. J. Setzler, C. A. Arrington, D. Lewis and J. T. Petty, *J. Phys. Chem. B*, 2023, **127**, 10851-10860.
45. D. Lewis, C. Setzler, P. M. Goodwin, K. Thomas, M. Branham, C. A. Arrington and J. T. Petty, *J. Phys. Chem. C*, 2023, **127**, 10574-10584.
46. Craig S. McKay and M. G. Finn, *Chemistry & Biology*, 2014, **21**, 1075-1101.
47. V. A. Bloomfield, D. M. Crothers and J. Tinoco, Ignacio, *Nucleic Acids: Structures, Properties, and Functions*, University Science Books, Sausalito, CA, 2000.
48. G. A. Crosby and J. N. Demas, *J. Phys. Chem.*, 1971, **75**, 991-1024.
49. C. He, P. M. Goodwin, A. I. Yunus, R. M. Dickson and J. T. Petty, *J. Phys. Chem. C*, 2019, **123**, 17588-17597.
50. J. T. Petty, M. Ganguly, A. I. Yunus, C. He, P. M. Goodwin, Y.-H. Lu and R. M. Dickson, *J. Phys. Chem. C*, 2018, **122**, 28382-28392.
51. S. M. Copp, P. Bogdanov, M. Debord, A. Singh and E. Gwinn, *Adv. Mater.*, 2014, **26**, 5839-5845.
52. B. Sengupta, C. M. Ritchie, J. G. Buckman, K. R. Johnsen, P. M. Goodwin and J. T. Petty, *J. Phys. Chem. C*, 2008, **112**, 18776-18782.
53. K. Koszinowski and K. Ballweg, *Chem. Eur. J.*, 2010, **16**, 3285-3290.
54. J. T. Petty, O. O. Sergev, M. Ganguly, I. J. Rankine, D. M. Chevrier and P. Zhang, *J. Am. Chem. Soc.*, 2016, **138**, 3469-3477.
55. S. M. Copp, D. Schultz, S. Swasey, J. Pavlovich, M. Debord, A. Chiu, K. Olsson and E. Gwinn, *J. Phys. Chem. Lett.*, 2014, **5**, 959-963.
56. J. T. Petty, O. O. Sergev, D. A. Nicholson, P. M. Goodwin, B. Giri and D. R. McMullan, *Anal. Chem.*, 2013, **85**, 9868-9876.
57. M. Ganguly, C. Bradsher, P. Goodwin and J. T. Petty, *J. Phys. Chem. C*, 2015, **119**, 27829-27837.
58. D. J. E. Huard, A. Demissie, D. Kim, D. Lewis, R. M. Dickson, J. T. Petty and R. L. Lieberman, *J. Am. Chem. Soc.*, 2019, **141**, 11465-11470.
59. L. D. Pachón, J. H. van Maarseveen and G. Rothenberg, *Advanced Synthesis & Catalysis*, 2005, **347**, 811-815.
60. J. Belloni, M. Mostafavi, H. Remita, J.-L. Marignier and a. Marie-Odile Delcourt, *New J. Chem.*, 1998, **22**, 1239-1255.
61. N. M. Dimitrijevic, D. M. Bartels, C. D. Jonah, K. Takahashi and T. Rajh, *J. Phys. Chem. B*, 2001, **105**, 954-959.
62. B. G. Ershov, E. Janata, A. Henglein and A. Fojtik, *J. Phys. Chem.*, 1993, **97**, 4589-4594.
63. M. L. Rodríguez-Sánchez, M. J. Rodríguez, M. C. Blanco, J. Rivas and M. A. López-Quintela, *J. Phys. Chem. B*, 2005, **109**, 1183-1191.
64. S. A. Mitchell, G. A. Kenney-Wallace and G. A. Ozin, *J. Am. Chem. Soc.*, 1981, **103**, 6030-6035.
65. V. O. Rodionov, S. I. Presolski, S. Gardinier, Y.-H. Lim and M. G. Finn, *J. Am. Chem. Soc.*, 2007, **129**, 12696-12704.
66. F. David, C. Setzler, A. Sorescu, R. L. Lieberman, F. Meilleur and J. T. Petty, *J. Phys. Chem. Lett.*, 2022, **13**, 11317-11322.
67. E. Boz and N. Ş. Tüzün, *Dalton Trans.*, 2016, **45**, 5752-5764.

Journal Name

ARTICLE

68. W. Wang, X.-Y. Zhai and L. Zhao, *Inorganic Chemistry*, 2023, **62**, 1414-1422.
69. R. Berg and B. F. Straub, *Beilstein Journal of Organic Chemistry*, 2013, **9**, 2715-2750.
70. V. Rück, V. A. Neacșu, M. B. Liisberg, C. B. Mollerup, P. H. Ju, T. Vosch, J. Kondo and C. Cerretani, *Adv. Opt. Mater.*, 2024, **12**, 2301928.
71. V. Rück, N. K. Mishra, K. K. Sørensen, M. B. Liisberg, A. B. Sloth, C. Cerretani, C. B. Mollerup, A. Kjaer, C. Lou, K. J. Jensen and T. Vosch, *J. Am. Chem. Soc.*, 2023, **145**, 16771-16777.
72. C. Cerretani, H. Kanazawa, T. Vosch and J. Kondo, *Angew. Chem. Int. Edit.*, 2019, **58**, 17153-17157.
73. J. T. Petty, M. Ganguly, I. J. Rankine, D. M. Chevrier and P. Zhang, *J. Phys. Chem. C*, 2017, **121**, 14936-14945.
74. M. S. Blevins, D. Kim, C. M. Crittenden, S. Hong, H.-C. Yeh, J. T. Petty and J. S. Brodbelt, *Acs Nano*, 2019, **13**, 14070-14079.
75. Y. Zhang, C. He, J. T. Petty and B. Kohler, *J. Phys. Chem. Lett.*, 2020, **11**, 8958-8963.

Data Availability Statement for

Click Catalysis and DNA Conjugation using a Nanoscale DNA/Silver Cluster Pair

Caleb J. Setzler^a and Jeffrey T. Petty^{a,*}

The data supporting this article have been included as part of the Supplementary Information.